

Unconventional Bose-Einstein condensations from spin-orbit coupling

Congjun Wu,¹ Ian Mondragon-Shem,^{1,2} and Xiang-Fa Zhou³

¹*Department of Physics, University of California, San Diego, CA 92093*

²*Instituto de Física, Universidad de Antioquia, AA 1226, Medellín, Colombia*

³*Key Laboratory of Quantum Information, University of Science and Technology of China, Hefei, Anhui 230026, China*

According to the “no-node” theorem, many-body ground state wavefunctions of conventional Bose-Einstein condensations (BEC) are positive-definite, thus time-reversal symmetry cannot be spontaneously broken. We find that multi-component bosons with spin-orbit coupling provide an unconventional type of BECs beyond this paradigm. We focus on the subtle case of isotropic Rashba spin-orbit coupling and the spin-independent interaction. In the limit of the weak confining potential, the condensate wavefunctions are frustrated at the Hartree-Fock level due to the degeneracy of the Rashba ring. Quantum zero-point energy selects the spin-spiral type condensate through the “order-from-disorder” mechanism. In a strong harmonic confining trap, the condensate spontaneously generates a half-quantum vortex combined with the skyrmion type of spin texture. In both cases, time-reversal symmetry is spontaneously broken. These phenomena can be realized in both cold atom systems with artificial spin-orbit couplings generated from atom-laser interactions and exciton condensates in semi-conductor systems.

PACS numbers: 71.35.-y, 73.50.-h, 03.75.Mn, 03.75.Nt

The conventional many-body ground state wavefunctions of bosons satisfy the celebrated “no-node” theorem in the absence of rotation, as written in Feynman’s textbook¹, which means that they are positive-definite in the coordinate representation. This theorem implies that time-reversal (TR) symmetry cannot be spontaneously broken. It applies to various ground states of bosons including Bose-Einstein condensates (BEC), Mott-insulating states, density-wave states, and super-solid states, thus making this a very general statement.

It would be exciting to search for novel types of quantum ground states of bosons beyond the “no-node” paradigm, such as unconventional BECs with complex-valued wavefunctions. This theorem does not apply to spinful bosons with spin-orbit (SO) coupling, whose linear dependence on momentum invalidates Feynman’s proof. Artificial SO coupling from laser-atom interactions have been applied to ultra-cold boson systems and its effects have been investigated.^{2–9} On the other hand, excitons in semiconductors^{10–13} exhibit SO coupling in their center-of-mass motion^{14–16}. In particular, exciting progress has been made in indirect exciton systems in coupled quantum wells where electrons and holes are spatially separate^{17,18}. The extraordinarily long life-time of indirect excitons provides a wonderful opportunity to investigate exciton condensation¹¹ with SO coupling.

In this article, we show that spin-orbit coupled bosons develop unconventional BECs beyond the “no-node” theorem. The Rashba SO coupled BEC with the spin-independent interaction exhibits frustration at the Hartree-Fock level. Quantum zero-point fluctuations select a coherent condensation in the presence of weak spatial inhomogeneities, which exhibits spiral spin-density waves and spontaneous TR symmetry breaking. In a strong external harmonic trap, the ground state condensate develops orbital angular momentum, which can be viewed as a half-quantum vortex. Moreover, the spin

density distribution exhibits a cylindrically symmetric spiral pattern as skyrmions.

We begin with a 3D two-component boson system with Rashba SO coupling in the xy -plane and with the contact spin-independent interaction, described by

$$H = \int d^3\vec{r} \, \psi_\alpha^\dagger \left\{ -\frac{\hbar^2 \nabla^2}{2M} - \mu \right\} \psi_\alpha + \hbar \lambda_R \psi_\alpha^\dagger \left\{ -i \nabla_y \sigma_x + i \nabla_x \sigma_y \right\} \psi_\beta + \frac{g}{2} \psi_\alpha^\dagger \psi_\beta^\dagger \psi_\beta \psi_\alpha, \quad (1)$$

where ψ_α is the boson operator; the pseudospin indices $\alpha = \uparrow, \downarrow$ refer to two different internal components of bosons; λ_R is the SO coupling strength which carries the unit of velocity; g describes the s -wave scattering interaction. Eq. (1) possesses a Kramer-type TR symmetry $T = i\sigma_2 C$ satisfying $T^2 = -1$, where C is the complex conjugate operation and σ_2 operates on the boson pseudospin degree of freedom.

In the homogeneous system, the single particle states are the helicity eigenstates of $\vec{\sigma} \cdot (\vec{k} \times \hat{z})$ with a dispersion relation given by $\epsilon_\pm(\vec{k}) = \frac{\hbar^2}{2M} [(k \mp k_{so})^2 + k_z^2]$ where $k_{so} = \frac{M\lambda_R}{\hbar}$. The energy minima are located on the lower branch along a ring with the radius k_{so} in the plane of $k_z = 0$. The corresponding two-component wavefunction $\psi_+(\vec{k})$ with $|k| = k_{so}$ can be solved as $\psi_+(\vec{k}) = \frac{1}{\sqrt{2}}(e^{-i\phi_k/2}, i e^{i\phi_k/2})^T$, where ϕ_k is the azimuth angle of the projection of \vec{k} in the xy -plane. The interaction part in Eq. (1) in the helicity basis can be represented as

$$H_{int} = \frac{g}{2} \sum_{\lambda\mu\nu\rho} \sum_{p_1 p_2 q} \langle \vec{p}_1 + \vec{q}; \lambda | \vec{p}_1; \rho \rangle \langle \vec{p}_2 - \vec{q}; \mu | \vec{p}_2; \nu \rangle \times \psi_\lambda^\dagger(\vec{p}_1 + \vec{q}) \psi_\mu^\dagger(\vec{p}_2 - \vec{q}) \psi_\nu(\vec{p}_2) \psi_\rho(\vec{p}_1), \quad (2)$$

where the Greek indices λ, ν, μ, ρ are the helicity indices \pm ; the matrix elements denote the inner product of spin

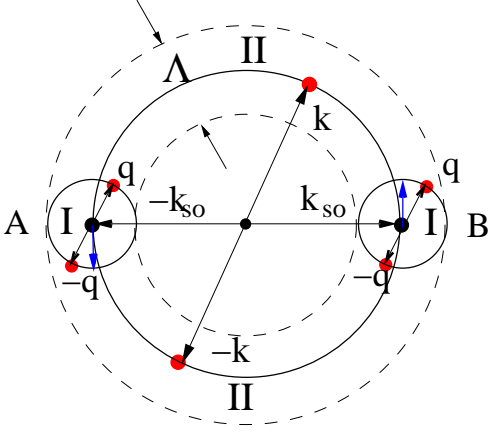


FIG. 1: The low energy ring with the radius k_{so} in momentum space. The coherent condensate involves points A and B with orthogonal spin polarizations. The low energy Bogoliubov excitations within $|k - k_{so}| < \Lambda$, $|k_z| < \Lambda$, and $\Lambda/k_{so} \ll 1$ are classified into two regimes I (inside two cylinders centering around A and B with radius of Λ) and II (outside).

wavefunctions of two helicity eigenstates at different momenta, e.g., $\langle \vec{p}_1 + \vec{q}; \lambda | \vec{p}_1; \rho \rangle = \frac{1}{2}[1 + \lambda \rho e^{i(\phi_{p1} - \phi_{p1+q})}]$.

The low energy Rashba ring brings degeneracy for the condensate configurations, *i.e.*, frustrations. Bosons tend to avoid the positive exchange energy for repulsive interactions, which is the driving force for BECs. Spin polarizations at two opposite ends of a diameter of the low energy ring are orthogonal to each other, and thus condensations with these states are free of exchange interactions. Without loss of generality, we define the fragmented and coherent condensates of Φ_{frag} and Φ_{coh} , respectively, as

$$\Phi_{frag} = \frac{1}{\sqrt{N_A! N_B!}} [\psi_+^\dagger(\vec{k}_A)]^{N_A} [\psi_+^\dagger(\vec{k}_B)]^{N_B} |0\rangle, \quad (3)$$

$$\Phi_{coh} = \frac{1}{\sqrt{N_0!}} \left\{ \sqrt{\frac{n_A}{n_0}} \psi_+^\dagger(\vec{k}_A) + e^{i\phi} \sqrt{\frac{n_B}{n_0}} \psi_+^\dagger(\vec{k}_B) \right\}^{N_0} |0\rangle \quad (4)$$

where A and B are points with $\vec{k}_A = (-k_{so}, 0, 0)$ and $\vec{k}_B = (k_{so}, 0, 0)$; (N_A, N_B) is the particle number partition satisfying $N_A + N_B = N_0$ with N_0 the total particle number in the condensate; $n_{A,B} = N_{A,B}/V$, and $n_0 = N_0/V$; the phase ϕ in Eq. 4 can be absorbed by the shift of the origin. At the Hartree-Fock level, Φ_{frag} and Φ_{coh} with an arbitrary partition $N_{A,B}$ have the same energy. Since fragmented condensates with different $N_{A,B}$ carry different momenta, they do not mix in the ideal homogeneous systems. However, even very weak spatial inhomogeneity can build up coherence among them, and leads to coherent condensates^{19,20}. Below we consider coherent condensates Φ_{coh} in Eq. 4, and leave a detailed study of the competition between fragmented and coherent condensates to a later work.

The zero-point quantum fluctuations lift the degeneracy among coherence condensates with different parti-

tions of $n_{A,B}$. We define a momentum scale k_{int} satisfying $\hbar^2 k_{int}^2 / (2M) = gn_0$ where gn_0 is the interaction energy scale. We only consider the limit of strong SO coupling, *i.e.*, $k_{in} \ll k_{so}$, and leave the general case for a later study. We chose an intermediate momentum cutoff Λ satisfying $k_{int} \ll \Lambda \ll k_{so}$, and study the Bogoliubov excitations in a cylindrical shell of

$$|\sqrt{k_x^2 + k_y^2} - k_{so}| < \Lambda, \quad |k_z| < \Lambda. \quad (5)$$

Within this shell, interaction energy is stronger than the kinetic energy, thus particle and hole states are significantly mixed. We further divide this shell into two parts I and II as depicted in Fig. 1. Part I is inside two cylinders with the radius of Λ centering around points A and B , and part II is outside these two cylinders.

For part I, we define boson operators in the lower branch as $a_{\vec{q}} = \psi_+(-k_{so}\hat{e}_x + \vec{q})$ and $b_{\vec{q}} = \psi_+(k_{so}\hat{e}_x + \vec{q})$, and $\langle a_{q=0} \rangle = \sqrt{N_a}$ and $\langle b_{q=0} \rangle = \sqrt{N_b}$, respectively. The low energy excitations in this region have been calculated in Ref. [9]. By defining $\gamma_1^\dagger(\vec{q}) = \frac{1}{\sqrt{N_0}}(\sqrt{N_a}a_{\vec{q}}^\dagger + \sqrt{N_b}b_{\vec{q}}^\dagger)$, $\gamma_2^\dagger(\vec{q}) = \frac{1}{\sqrt{N_0}}(\sqrt{N_b}a_{\vec{q}}^\dagger - \sqrt{N_a}b_{\vec{q}}^\dagger)$, the mean-field Hamiltonian, up to the order of q^2 , is represented as

$$H_{MF,1} = \sum_{\vec{q}} \left\{ E(\vec{q}) \gamma_1^\dagger(\vec{q}) \gamma(\vec{q}) + gn_0 [\gamma_1^\dagger(\vec{q}) \gamma_1^\dagger(-\vec{q}) + h.c.] + E(\vec{q}) \gamma_2^\dagger(\vec{q}) \gamma_2(\vec{q}) \right\}, \quad (6)$$

where $E(\pm\vec{q}) \approx \hbar(q_x^2 + q_z^2)/(2M)$ up to the order of $O(q^3/k_{so})$. The Bogoliubov modes mixing $\gamma_1^\dagger(\vec{q})$ and $\gamma_1(-\vec{q})$ exhibit the spectrum of $\hbar\omega(\vec{q}) = \sqrt{E_{\vec{q}}(E_{\vec{q}} + 2gn_0)} \approx \sqrt{\frac{\hbar gn_0}{M}} \sqrt{q_x^2 + q_z^2}$. This is the phonon mode describing the overall density fluctuations, which exhibits linear dispersion relation for \vec{q} in the xz -plane and becomes soft for \vec{q} along \hat{e}_y . The γ_2 mode represents the relative density fluctuations between two condensates which describes spin wave excitations. This mode remains a free particle spectrum $E(\vec{q})$. Both of the $\gamma_{1,2}$ modes only depend on the total condensation fraction N_0 . Hence, the contribution from part I does not lift the degeneracy between different partitions of (N_A, N_B) up to the quadratic order of q .

Next we turn to the Bogoliubov spectra in part II where $\psi_+(\vec{k})$ is degenerate with $\psi_-(-\vec{k})$ but not with $\psi_+(2\vec{k}_{A,B} - \vec{k})$. The mean-field Hamiltonian reads

$$H_{MF,2} = \sum_{\vec{k}} \psi_+^\dagger(\vec{k}) \psi_+(\vec{k}) \left\{ \epsilon(\vec{k}) + \frac{g}{2}(n_0 - \Delta n \cos \phi_k) \right\} + g\sqrt{n_a n_b} \left\{ \psi_+^\dagger(\vec{k}) \psi_-^\dagger(-\vec{k}) \cos \phi_{\vec{k}} e^{i\phi_{\vec{k}}} + h.c. \right\}, \quad (7)$$

where $\Delta n = n_a - n_b$. The Bogoliubov spectra can be solved as $H_{MF,2} = \sum_{\vec{k}} \left\{ \omega(\vec{k}) (\gamma_3^\dagger(\vec{k}) \gamma_3(\vec{k}) + \frac{1}{2}) \right\}$ with

$$\omega(k) = \sqrt{\epsilon_{\vec{k}}(\epsilon_{\vec{k}} + gn_0) + \frac{g^2 n_0^2}{4} f(x) + \frac{gn_0}{2} x \cos \phi_k}, \quad (8)$$

where $x = \Delta n/n_0$ and $f(x) = \sin^2 \phi_k + x^2 \cos^2 \phi_k$. The second term in Eq. 8 averages to zero, and thus the total zero-point energy in regime II depends on x^2 . It reaches the minimum at $x = 0$, or, $n_a = n_b$, which describes a spin-density-wave spiral in the xz -plane with the condensate wavefunction as

$$\psi_{cond} = (\cos k_{so}x, \sin k_{so}x)^T. \quad (9)$$

An accurate evaluation of the zero-point energy needs to deal with the ultraviolet divergence of the integral over momentum space, which will be postponed to a later publication.

The above “order-from-disorder” results can be captured from constructing an effective Gross-Pitaevskii (GP) equation. Generally speaking, the interaction parameters in the GP equation are renormalized from their bare values in Eq. 1 by the zero-point motions. Because the kinetic energy only possesses the $SO(2)$ rotational symmetry, although the bare interaction is spin-independent, an extra spin-dependent term should be generated as

$$g' [n_{\uparrow}(\vec{r}) - n_{\downarrow}(\vec{r})]^2, \quad (10)$$

where $n_{\uparrow, \downarrow}$ are particle densities of two spin components. Obviously, $g' < 0$ selects the spin-spiral condensate involving the s_z component (e.g. Eq. 9) even though the total s_z averages to zero, while $g' > 0$ selects the plane-wave condensate with spin polarization in the xy -plane (e.g. $\psi_{cond} = \frac{1}{\sqrt{2}} e^{ik_{so}x} (1, i)^T$). According to the result of Eq. 9, we conclude that $g' < 0$ is the case for Eq. 1. Furthermore, g' is at the order of g^2 from the power-counting of the integral of the zero-point energy. The usual leading order correction to the interaction parameter in 3D BECs is of $g^{\frac{5}{2}}$. This difference is due to the effective dimension reduction by the Rashba ring.

Next we consider the situation of a strong confining potential $V_{ex}(r) = \frac{1}{2} M \omega_T^2 (x^2 + y^2)$ and a relatively weak interaction. The condensate along the z -axis is set uniform. In this case, the single particle energy dominates over the interaction energy, which mixes the plane-wave states along the low energy ring. We define the SO energy scale $E_{so} = \hbar \lambda_R / l$ where $l = \sqrt{\hbar / (M \omega_T)}$ is the length scale of the trap, and the dimensionless parameter $\alpha = E_{so} / (\hbar \omega_T) = l k_{so}$. Let us gain some intuition in the strong SO limit $\alpha \gg 1$. The harmonic potential in the momentum representation becomes $V_{ex} = \frac{1}{2} M \omega_T^2 (i \partial_{\vec{k}} - \vec{A}(\vec{k}))^2$, where $\vec{A}(\vec{k}) = i \langle \psi_{\uparrow}(\vec{k}) | \partial_{\vec{k}} | \psi_{\uparrow}(\vec{k}) \rangle$ carrying a π -flux located at $\vec{k} = (0, 0)$. V_{ex} quantizes the orbital motion around the ring as

$$\Delta E_{m+\frac{1}{2}} = \frac{1}{2} M \omega_T^2 \left(\frac{m+\frac{1}{2}}{k_{so}} \right)^2 = \frac{1}{2\alpha^2} \hbar \omega_T (m + \frac{1}{2})^2. \quad (11)$$

The single particle ground state forms the Kramer doublets corresponding to $m + \frac{1}{2} = \pm \frac{1}{2}$. Equivalently, in the real space, due to the 2D rotational symmetry, the

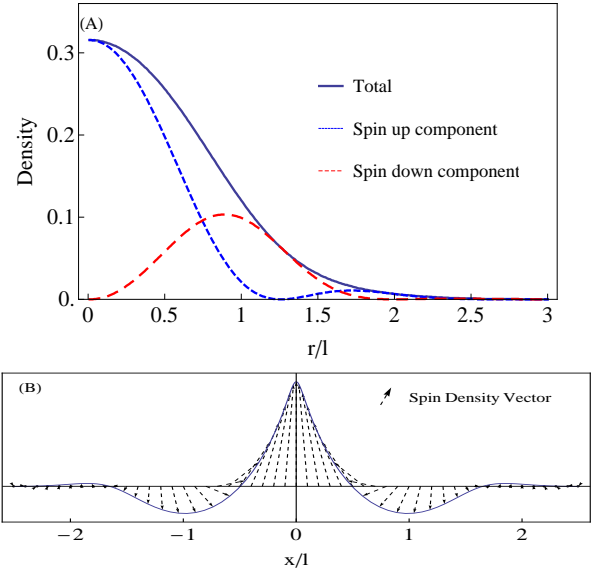


FIG. 2: (A) The radial density distribution of spin up and down components, and the total density distribution in the unit of N_0 at $\alpha = 2$ and $\beta = 5$. (B) The skyrmion type spin texture configuration plotted in the xz -plane.

wavefunctions can be denoted by the total angular momentum $j_z = m + \frac{1}{2}$. The ground state single particle wavefunctions form a Kramer doublet as represented in cylindrical coordinates as

$$\psi_{\frac{1}{2}} = \begin{pmatrix} f(r) \\ g(r)e^{i\phi} \end{pmatrix}, \quad \psi_{-\frac{1}{2}} = \begin{pmatrix} -g(r)e^{-i\phi} \\ f(r) \end{pmatrix}, \quad (12)$$

where $f(r)$ and $g(r)$ are real functions. At $\alpha \gg 1$, these doublet states have nearly equal weight in the spin up and down components, i.e., $\int dr d\phi r |f(r)|^2 \approx \int dr d\phi r |g(r)|^2$, thus the spin moment averages to zero. In the presence of weak interactions, bosons condense into one of the TR doublets, the average orbital angular momentum per particle is $\hbar/2$, i.e., one spin component stays in the s -state and the other one in the p -state. This is a half-quantum vortex configuration spontaneously breaking TR symmetry^{21–23}.

We have performed numerical calculation to confirm the above intuitive picture. The characteristic interaction energy scale is defined as $E_{int} = g N_0 / (\pi l^2 L_z)$, where L_z is the system size along the z -axis, and the dimensionless parameter $\beta = E_{int} / (\hbar \omega_T)$. We numerically solve the GP equation

$$\left\{ -\frac{\hbar^2 \nabla^2}{2M} + \hbar \lambda_R (-i \nabla_y \sigma_{x, \alpha\beta} + i \nabla_x \sigma_{y, \alpha\beta}) + g n(r, \phi) + \frac{1}{2} M \omega_T^2 r^2 \right\} \psi_\beta(r, \phi) = E \psi_\alpha(r, \phi), \quad (13)$$

where $n(r, \phi)$ is the particle density. The parameter values are chosen as $\alpha = 2$ and $\beta = 5$. The interaction effectively weakens the harmonic potential and does not change the orbital partial wave structure of the wavefunctions. We show the radial density profiles of both

spin components $|f(r)|^2$ and $|g(r)|^2$ in Fig. 2 A. Each of them exhibits oscillations at a pitch value of approximately $2k_{so}$, which originate from the low energy ring structure and, thus, are analogous to the Friedel oscillations in fermion systems. The spin density, defined as $\vec{S}(r, \phi) = \psi_\alpha^*(r, \phi) \vec{\sigma}_{\alpha\beta} \psi_\beta(r, \phi)$, exhibits an interesting topological spin texture configuration. Let us first look at its distribution along the x -axis where the supercurrent is along the y -direction and the spin lies in the xz -plane. Explicitly, we express $S_z(r, \phi) = \frac{1}{2}(|f(r)|^2 - |g(r)|^2)$ and $S_x(r, \phi) = f(r)g(r)$. The radial oscillations of $|f(r)|^2$ and $|g(r)|^2$ have an approximate π phase shift, which arises from the different angular symmetries. As a result, \vec{S} spirals in the xz -plane along the x -axis as plotted in Fig. 2 B at the pitch value of the density oscillations. The spin density distribution in the whole space can be obtained through a rotation around the z -axis, which exhibits the skyrmion configuration.

Because of the non-linearity of the GP equation, the superposition principle, generally speaking, does not apply. Nevertheless, if we only keep the $SU(2)$ invariant interaction term in the GP equation, all of the linear superpositions of the Kramer doublet $\psi_{\pm\frac{1}{2}}$ in Eq. 12 can rotate into one another, thus are degenerate. Therefore, in real experiment systems, if the initial state is prepared with total angular momentum $j_z = 0$, we will obtain a superposition of $\psi_{\pm\frac{1}{2}}$ due to the conservation of j_z . On the other hand, if the initial state is prepared with the average j_z per particle $\pm\frac{1}{2}$, say, by cooling down from the fully polarized spin up or down state, then $\psi_{\pm\frac{1}{2}}$ will be reached. We also remind that if we go beyond the Hartree-Fock level to include the zero-point motion correction, the extra spin-dependent term of Eq. 10 will also lift the above accidental degeneracy.

So far we have presented two different types of condensations. The half-quantum vortex condensate preserves rotational symmetry, which is favored by the trapping potential and is stable for weak interaction strengths. Instead, the spin-spiral condensate involving two plane-waves with opposite wavevectors breaks rotational symmetry. It is favored by interactions, and should survive under weak trapping potentials. Or, equivalently, with fixing α , it can be stabilized by increasing the interaction energy scale β . We have performed the numerical study for the critical line between them as presented in Fig. 3. For simplicity, the spin-independent interaction is still used. We calculate the expectation value of $\langle G | j_z^2 | G \rangle$ of the condensate wavefunction. In regime I, the condensate is chosen as the eigenstate with $j_z = \frac{1}{2}(-\frac{1}{2})$ and thus $\langle G | j_z^2 | G \rangle = \frac{1}{4}$. In regime II, $\langle G | j_z^2 | G \rangle$ deviates from $\frac{1}{4}$. The condensate starts to involve high angular momentum components, and thus breaks rotational symmetry. It is qualitatively in the same phase of spin-spiral condensate with cylindrical boundary condition.

The recent research focus of the “synthetic gauge fields” in cold atom systems provides a promising method to observe the above exotic SO coupled BECs^{5–8,25}. In

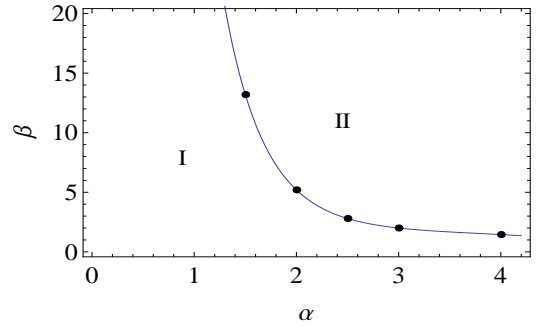


FIG. 3: The phase diagram boundary of β_c v.s α between (I) the half-quantum vortex condensate and (II) spin-spiral condensate. The transition from (I) to (II) breaks rotational symmetry.

particular, anisotropic SO coupled BEC has been realized experimentally⁸. Furthermore, several proposals of realizing isotropic Rashba SO coupling have appeared^{4,25,34}. A typical set of parameter values are provided in Ref.⁴ for a trap frequency $\omega_T = 2\pi \times 10$ Hz, a characteristic Rabi frequency $\Omega = 2\pi \times 10^7$ Hz, and a detuning $\Delta = 2\pi \times 10^{11}$ Hz, which satisfy $\omega_T \ll \Omega \ll \Delta$ and $\omega_T \ll \Omega^2/\Delta$. The value of α can vary from 0 up to the order of several tens. With the typical particle number $N_0 = 10^6$, the interaction energy scale E_{int} is around $100nK$, or 2 kHz²⁶, and β is of the order of several tens. Thus for the most convenient experimental parameters, the spin-spiral condensate is realized. Nevertheless, the half-quantum vortex condensate can be realized by reducing the condensate particle number by one order to $N_0 = 10^5$ combined with increasing the trap frequency. The detection would be straightforward as performed in previous time-of-flight imaging in vortex experiments^{27,28}. By separately imaging the density profiles of the pseudospin up and down components in the time-of-flight spectra²⁷, the radial oscillation of the S_z component can be directly seen.

Another class of SO coupled boson systems are the indirect excitons in 2D coupled double quantum wells. Both electrons and holes possess relativistic SO coupling and so does the center of mass motion of excitons. The real space spin configurations of exciton condensations can be conveniently detected through photoluminescence from electro-hole recombination. Excitingly, the recent experiment has observed spin-textures of the coherent exciton systems which arise from SO coupling and exhibit a similar pattern shown in Fig. 2³⁰. We leave a detailed study on this phenomenon to a future paper.

In summary, we find that bosons with SO coupling exhibit complex-valued condensations beyond Feynman’s “no-node” paradigm. The coherent spin-spiral BEC is realized when interaction energy is dominant, while the half-quantum vortex BEC is stable when the trapping potential is strong. The half-quantum vortex condensate also exhibits the skyrmion type topological spin-texture configuration.

C. W. is supported by U.S. NSF-DMR1105945 and AFOSR-YIP program. X. F. Z. acknowledges the support of CUSF, SRFDP (20103402120031), and the China Postdoctoral Science. C. W. thanks helpful discussions with L. Butov, L. M. Duan, M. Fogler, J. Hirsch, T. L.

Ho, L. Sham, S. C. Zhang, and F. Zhou.

Note added: After the three version of this manuscript was posted on arXiv, there appeared two experimental works of SO coupled BECs in both cold atom and exciton systems^{8,30}, and several theoretical investigations^{31–36}.

-
- ¹ R. P. Feynman, *Statistical Mechanics, A Set of Lectures* (Addison-Wesley Publishing Company, ADDRESS, 1972).
 - ² G. Juzeliunas *et al.*, Phys. Rev. Lett. **100**, 200405 (2008).
 - ³ J. Y. Vaishnav and C. W. Clark, Phys. Rev. Lett. **100**, 153002 (2008).
 - ⁴ T. D. Stanescu, C. Zhang, and V. Galitski, Phys. Rev. Lett. **99**, 110403 (2007).
 - ⁵ Y.-J. Lin *et al.*, Phys. Rev. Lett. **102**, 130401 (2009).
 - ⁶ Y.-J. Lin *et al.*, Nature **462**, 628 (2009).
 - ⁷ I. B. Spielman, Phys. Rev. A **79**, 063613 (2009).
 - ⁸ Y. J. Lin, K. Jimenez-Garcia, and I. B. Spielman, Nature **471**, 83 (2011).
 - ⁹ T. Stanescu, B. Anderson, and V. Galitski, Phys. Rev. A **78**, 023616 (2008).
 - ¹⁰ D. W. Snoke, J. P. Wolfe, and A. Mysyrowicz, Phys. Rev. B **41**, 11171 (1990).
 - ¹¹ L. V. Butov, J. Phys.: Cond. Matt. **16**, R1577 (2004).
 - ¹² L. V. Butov, J. Phys.: Cond. Matt. **19**, 295202 (2007).
 - ¹³ L. A. V. Timofeev *et al.*, J. Phys.: Cond. Matt. **19**, 295209 (2007).
 - ¹⁴ T. Hakioglu and M. Sahin, Phys. Rev. Lett. **98**, 166405 (2007).
 - ¹⁵ M. A. Can and T. Hakioglu, arXiv:0808.2900, 2008.
 - ¹⁶ W. Yao and Q. Niu, Phys. Rev. Lett. **101**, 106401 (2008).
 - ¹⁷ L. V. Butov *et al.*, Phys. Rev. Lett. **73**, 304 (1994).
 - ¹⁸ L. V. Butov, A. C. Gossard, and D. S. Chemla, Nature **418**, 751 (2002).
 - ¹⁹ E. J. Mueller, T. L. Ho, M. Ueda, and G. Baym, Phys. Rev. A **74**, 33612 (2006).
 - ²⁰ T. L. Ho and S. K. Yip, Phys. Rev. Lett. **84**, 4031 (2000).
 - ²¹ M. M. Salomaa and G. E. Volovik, Phys. Rev. Lett. **55**, 1184 (1985).
 - ²² C. Wu, J. P. Hu, and S. C. Zhang, Int. J. Mod. Phys. B **V24**, 311 (2010).
 - ²³ F. Zhou, Int. Jour. Mod. Phys.B, **17** **17**, 2643 (2003).
 - ²⁴ J. Larson and E. Sjöqvist, Phys. Rev. A **79**, 043627 (2009).
 - ²⁵ D. L. Campbell, G. Juzeliunas, and I. B. Spielman, arXiv:1102.3945.
 - ²⁶ A. J. Leggett, Rev. Mod. Phys. **73**, 307 (2001).
 - ²⁷ K. W. Madison, F. Chevy, W. Wohlleben, and J. Dalibard, Phys. Rev. Lett. **84**, 806 (2000).
 - ²⁸ B. P. Anderson, P. C. Haljan, C. E. Wieman, and E. A. Cornell, Phys. Rev. Lett. **85**, 2857 (2000).
 - ²⁹ M. Z. Maialle, E. A. de Andrada e Silva, and L. J. Sham, Phys. Rev. B **47**, 15776 (1993).
 - ³⁰ A. A. High, *et al.*, arXiv:1103.0321.
 - ³¹ T. L. Ho, S. Z. Zhang, arXiv:1007.0650.
 - ³² C. Wang, C. Gao, C. M. Jian, H. Zhai, Phys. Rev. Lett., **105**, 160403 (2010).
 - ³³ S. K. Yip, arXiv:1008.2263.
 - ³⁴ Y. Zhang, L. Mao, C. W. Zhang, arXiv:1102.4045.
 - ³⁵ Z. F. Xu, R. Lv, L. You, Phys. Rev. A **83**, 053602 (2011).
 - ³⁶ T. Kawakami, T. Mizushima, K. Machida, arXiv:1104.4179.